Mechanistic Studies of Reactions of Peroxodiiron(III) Intermediates in T201 Variants of Toluene/o-Xylene Monooxygenase Hydroxylase

Published in final edited form as:
Biochemistry. 2011 June 14; 50(23): 5391–5399. doi:10.1021/bi200340f.

Mechanistic Studies of Reactions of Peroxodiiron(III) Intermediates in T201 Variants of Toluene/*o*-Xylene Monooxygenase Hydroxylase[†]

Woon Ju Song and **Stephen J. Lippard**[*]
Department of Chemistry, Massachusetts Institute of Technology, Cambridge, Massachusetts 02139

Abstract

Site-directed mutagenesis studies of a strictly conserved T201 residue in the active site of toluene/*o*-xylene monooxygenase hydroxylase (ToMOH) revealed that a single mutation can facilitate kinetic isolation of two distinctive peroxodiiron(III) species, designated $T201_{peroxo}$ and $ToMOH_{peroxo}$, during dioxygen activation. Previously we characterized both oxygenated intermediates by UV-vis and Mössbauer spectroscopy, proposed structures from DFT and QM/MM computational studies, and elucidated chemical steps involved in dioxygen activation through the kinetic studies of $T201_{peroxo}$ formation. In the current study, we investigated the kinetics of $T201_{peroxo}$ decay to explore the reaction mechanism of the oxygenated intermediates following O_2 activation. The decay rates of $T201_{peroxo}$ were monitored in the absence and presence of external (phenol) or internal (tryptophan residue in an I100W variant) substrates under pre-steady-state conditions. Three possible reaction pathways were evaluated and the results demonstrate that $T201_{peroxo}$ is on the pathway of arene oxidation and appears to be in equilibrium with $ToMOH_{peroxo}$.

Bacterial multicomponent monooxygenases (BMMs)[1] are capable of activating dioxygen and catalyzing selective organic substrate oxidation (1, 2). The BMMs contain carboxylate-bridged non-heme diiron centers, now a common motif in metalloenzymes (3) including ribonucleotide reductases (4), desaturases (5), *myo*-inositol oxygenase (6), human deoxyhypusine hydroxylase (7), amine oxy-genase (8), and a recently characterized enzyme on the ubiquinone biosynthesis pathway (9). Studies of BMMs have mainly focused on soluble methane monooxygenase hydroxylase (sMMOH), revealing two peroxodiiron(III) (P* and P or H_{peroxo}) and a diiron(IV) species (Q) that are generated during dioxygen activation in the presence of a regulatory protein (MMOB) (10–15). Recently, we have been investigating the toluene/*o*-xylene monooxygenase hydroxylase (ToMOH) component of

[†]This work was funded by grant GM032134 from the National Institute of General Medical.

[*]To whom correspondence should be addressed. lippard@mit.edu. Telephone: (617) 253-1892. Fax: (617) 258-8150.

SUPPORTING INFORMATION AVAILABLE. Table S1 and Figure S1–S2. This material is available free of charge via the Internet at http://pubs.acs.org.

[1]Abbreviations: BMMs, bacterial multicomponent monooxygenases; DFT, density functional theory; EPR, electron paramagnetic resonance; k_{decay}, decay rate constant; k_{form}, formation rate constant; KIE, kinetic isotope effect; KSIE, kinetic solvent isotope effect; sMMOB, regulatory protein of soluble methane monooxygenase; sMMOH, hydroxylase component of soluble methane monooxygenase; MOPS, 3-(*N*-morpholino)propanesulfonic acid; P or H_{peroxo}, second peroxodiiron intermediate of sMMOH; P*, first peroxodiiron intermediate of sMMOH; Q, di(μ-oxo)diiron(IV) intermediate of sMMOH; QM/MM, quantum mechanics/molecular mechanics; RFQ, rapid freeze quench; $T201_{peroxo}$, peroxodiiron(III) intermediates observed in T201 variants; $T201_{peroxo}$*, an intermediate generated in the decomposition pathway of $T201_{peroxo}$; ToMO, toluene/*o*-xylene monooxygenase; ToMOD, regulatory protein of ToMO; ToMOH, hydroxylase component of ToMO; $ToMOH_{ox}$, resting state of ToMOH; $ToMOH_{red}$, reduced ToMOH; $ToMOH_{red}$D, reduced ToMOH in complex with ToMOD; $ToMOH_{peroxo}$, diiron(III) intermediate observed in the wild-type ToMOH enzyme

toluene/*o*-xylene monooxygenase (ToMO), which evolved from an ancestor similar to that of sMMOH (16, 17). Because the two hydroxylases share very similar diiron active site structures (18), it seemed plausible that their dioxygen activation mechanisms might proceed through analogous peroxodiiron(III)- and Q-type intermediates. Pre-steady-state studies of dioxygen activation by ToMOH in the presence of its cognate regulatory protein ToMOD (hereafter $ToMOH_{red}D$), however, revealed that this enzyme system generates a previously unprecedented diiron(III) intermediate, $ToMOH_{peroxo}$ (Chart 1A) (19). Moreover, no evidence for formation of a Q-like species has yet been identified in ToMOH reactions. These results imply that ToMOH has a different O_2 activation profile from that of sMMOH, oxidizing its substrates via different intermediates.

Pre-steady-state studies of dioxygen activation in ToMOH are hampered by the absence of an optical band in the $ToMOH_{peroxo}$ intermediate. By perturbing the active site structure through the generation of Ser, Cys, and Gly variants of ToMOH T201, however, a residue strictly conserved and located close to the diiron centers in all BMMs, we discovered a novel intermediate, $T201_{peroxo}$. This species forms in addition to $ToMOH_{peroxo}$ in these variants (20, 21). $T201_{peroxo}$ exhibits UV-vis and Mössbauer spectra similar to those of H_{peroxo} in sMMOH (Chart 1B), and its optical feature allowed us to obtain kinetic parameters of its formation by stopped-flow spectroscopy in the T201 variants under a variety of reaction conditions. Formation rates of $T201_{peroxo}$ in the T201S variant are proportional to the concentration of O_2, a result that allowed us to determine the likely pathway by which dioxygen accesses the active site diiron center (22). DFT and QM/MM calculations, revealed how the conformation of the side chain at T201 site perturbs the energetics of two oxygenated species $ToMOH_{peroxo}$ and $T201_{peroxo}$ (23). Our studies further suggested that that proton transfer to either the peroxo unit or an adjacent shifting carboxylate ligand (E231) during dioxygen activation can determine the geometry of oxygenated dii-ron(III) intermediates as either $ToMOH_{peroxo}$ or $T201_{peroxo}$, respectively (Chart 1B) (21).

Although accurate stopped-flow kinetic parameters for the formation and decay of $ToMOH_{peroxo}$ could not be measured in the T201S variant, time-dependent Mössbauer spectra obtained from freeze-quench investigations of its reaction with O_2 in the presence of ToMOD revealed values comparable to those previously obtained with the wild-type enzyme (20). The data suggested that $T201_{peroxo}$ and To-MOH_{peroxo} are generated by separate pathways (19, 20), with $T201_{peroxo}$ forming more rapidly than To-MOH_{peroxo}, their respective rate constants being $k_{form} = 85 \pm 11\ s^{-1}$ vs. $\sim 26\ s^{-1}$ at 4 °C, pH 7.0. Moreover, the decay rate constant of $T201_{peroxo}$ at this temperature ($2.9\ s^{-1}$) is much less than k_{form} of $ToMOH_{peroxo}$ ($\sim 26\ s^{-1}$), further consistent with $T201_{peroxo}$ and $ToMOH_{peroxo}$ forming by separate pathways during di-oxygen activation.

To further probe the properties of $T201_{peroxo}$ and $ToMOH_{peroxo}$ in T201 variants of ToMOH, we explored in the present study three plausible scenarios: (i) that $T201_{peroxo}$ and $ToMOH_{peroxo}$ are formed and react consecutively; (ii) that $T201_{peroxo}$ and $ToMOH_{peroxo}$ form and react independently; (iii) that $T201_{peroxo}$ and $ToMOH_{peroxo}$ are in equilibrium, with one dominating subsequent reactivity. From the kinetics of the reaction of $T201_{peroxo}$ with arene substrates, following by monitoring changes in its optical spectrum, we were able to evaluate these three working models for formation and decay of $T201_{peroxo}$ and $ToMOH_{peroxo}$ and to identify the arene-oxidizing intermediate(s). Aromatic hydroxylation by $T201_{peroxo}$ was monitored in the three T201 variants, T201S, T201C, and T201G, previously determined to form the intermediate, although with distinct kinetics. These experiments were conducted with the use of phenol as an external substrate or by converting I100, a residue in close proximity to the active site, into tryptophan as an internal substrate. In addition to the kinetic studies of $T201_{peroxo}$, the amount of the oxidized phenol or I100W

was quantitated in the three T201 variants to further explore the role of T201 during catalysis.

EXPERIMENTAL PROCEDURES

General Considerations

Plasmids containing the genes for expressing toluene/*o*-xylene monooxygenase components were supplied by the laboratory of Professor Alberto Di Donato, Naples, Italy. All ToMO components and ToMOH T201X mutants (X= S, C, G) were prepared as described previously (20, 24). I100W/T201X double mutants (X= S, C, G, V) were obtained by using the pET22b(+)/touBEA T201X vector with I100W primers (5′-CAA CTT CAC TTC GGA GCG TGG GCA CTT GAA GAA TAC G-3′ and 5′-C GTA TTC TTC AAG TGC CCA CGC TCC GAA GTG AAG TTG-3′). DNA sequences were confirmed by the MIT-BioPolymers Laboratory. Vectors were transformed into *E. coli* strain BL21(DE3) cells for protein expression. Cell growth and protein purification procedures were as same as for the wild type enzyme. An iron assay was performed, as described previously (19, 24).

Kinetic Studies of Oxygenated Intermediates in T201X/I100W (X= S, G, C, V)

UV-vis spectra of $T201_{peroxo}$ (20, 21) and I100W-radical species (25) were monitored as described. Optical bands originating from $T201_{peroxo}$ and the I100W-radical were monitored by using a HiTech DX2 stopped-flow spectrophotometer. The drive syringes and flow lines of this instrument were made anaerobic by passage of at least 10 mL of anaerobic solution of 4 mM sodium dithionite in 25 mM MOPS, pH 7 buffer. The excess dithionite was removed by flushing the syringes with anaerobic buffer. T201X or T201X/I100W ToMOH proteins were reduced anaerobically by reacting the protein with excess sodium dithionite in the presence of an equimolar amount of methyl viologen for 10 min. The reduced protein ($ToMOH_{red}$) was dialyzed against 1 L of 25 mM MOPS, pH 7.0 buffer for ~ 3 hr, anaerobically. Following dialysis, the regulatory protein (ToMOD) was added to the reduced ToMOH. The solution was transferred to a tonometer and loaded into the anaerobic stopped flow instrument. This solution was rapidly mixed against an equal volume of O_2-saturated 25 mM MOPS, pH 7.0 buffer. The temperature was thermostatted at 4 °C using a circulating water bath. Time-dependent optical changes at wavelengths corresponding to the formation and decay of $T201_{peroxo}$ (675 nm) and to the I100W-radical species (500 nm) were collected using a PMT (photomultiplier tube) following halogen lamp illumination or a diode-array with a xenon lamp. Data were analyzed by the software packages Kinetic Studio (TgK Scientific) and Origin 6.1 (OriginLab Corporation) as described previously (15, 20, 26). For the T201S and T201G ToMOH variants, an analytical function derived from a model $ToMOH_{red} \rightarrow T201_{peroxo} \rightarrow ToMOH_{ox}$ was applied to obtain formation and decay rate constants for $T201_{peroxo}$. For the T201C variant, an analytical function corresponding to the model $ToMOH_{red} \rightarrow T201_{peroxo} \rightarrow T201_{peroxo}^{*} \rightarrow ToMOH_{ox}$ was derived to measure the formation and two decay rate constants of $T201_{peroxo}$. In the T201X/I100W variants, the formation and decay of the $T201_{peroxo}$ and I100W-radical species were fit to analytical functions derived for $To\text{-}MOH_{red} \rightarrow T201_{peroxo} \rightarrow ToMOH_{ox}$ and I100W-radical precursor → I100W-radical → oxidized product of I100W models, respectively.

Kinetics of an Oxygenated Intermediate in the Reactions with Arene Substrates

The arene substrate phenol was dissolved in dioxygen-saturated buffer and the solution was rapidly mixed with $ToMOH_{red}$D in a single-mixing stopped flow spectrophotometer at 4 °C. Time-dependent optical changes arising from the formation and decay of $T201_{peroxo}$ were then analyzed, as described previously (21).

For a kinetic isotope effect (KIE) measurement, phenol-2,3,4,5,6-d_5 (hereafter phenol-d_5) (98 atom % D) purchased from Sigma-Aldrich was used without further purification. For kinetic solvent isotope effect (KSIE) measurements, deuterium oxide (99.9 atom % D) purchased from Cambridge Isotope Laboratories or Icon Isotopes was used to prepare 25 mM MOPS buffer, pL 7.0. The pL value was adjusted by adding an appropriate amount of NaOD solution (Aldrich). Dioxygen activation of ToMOH was monitored at 5 °C, which was thermostatted using a circulating water bath.

RESULTS AND DISCUSSION

Decay of T201$_{peroxo}$ in the Presence of Aromatic Substrates

To determine whether T201$_{peroxo}$ is kinetically competent to hydroxylate aromatic substrates, its formation and decay rates were monitored in the presence of phenol. Phenol was selected as substrate because the natural substrates, toluene and *o*-xylene, are less soluble in water. In addition, ToMO displays a high steady state activity with phenol (19). To observe its effects on the decay rate of T201$_{peroxo}$, phenol was dissolved in dioxygen-saturated buffer and rapidly mixed with the same volume of a solution containing reduced T201X ToMOH and ToMOD. Changes in absorbance at 675 nm, corresponding to formation and decay of T201$_{peroxo}$, were monitored using stopped-flow optical spectroscopy (Figure 1). The rate constants were then obtained by the fit to an analytical function derived from a model involving two consecutive, irreversible steps.

In the reaction of phenol and dioxygen with the T201S variant of ToMOH$_{red}$D, the formation rate of T201$_{peroxo}$ was unaltered over a 0 – 25 mM range of phenol concentrations (Figure 2A). This result indicates that the substrate does not alter the mechanism of dioxygen activation to form T201$_{peroxo}$. The presence of phenol, however, accelerated the decay of T201$_{peroxo}$, thereby diminishing the accumulation of this intermediate (Figure 1A). Because the decay rate of T201$_{peroxo}$ in the presence of phenol is much faster than the rate of catechol production measured under steady-state conditions (20), it is apparent that T201$_{peroxo}$ is kinetically competent for, and probably on the pathway to, phenol oxidation. A plot of k_{decay} versus phenol concentration yielded a linear relationship, from which we could derive a second-order rate constant of 0.18 ± 0.02 s^{-1} mM^{-1} (Figure 2A).

T201$_{peroxo}$ is also observed during dioxygen activation of the T201C and T201G variants of To-MOH. T201$_{peroxo}$ reacts in a similar manner with phenol in the T201C and T201G ToMOH variants. In the absence of arene substrate, T201$_{peroxo}$ in T201C variant decays by two consecutive process, T201$_{peroxo}$ → T201$_{peroxo}$* → ToMOH$_{ox}$. Two decay rate constants, k_{decay1} and k_{decay2}, corresponding to the conversion of T201$_{peroxo}$ to T201$_{peroxo}$* and of T201$_{peroxo}$* to ToMOH$_{ox}$, were obtained. The change in the absorbance of T201$_{peroxo}$ at 675 nm in T201C variant was recorded in the absence and presence of arene substrate (Figure 1B). As described above for the T201S variant, formation rate of T201$_{peroxo}$ was independent of phenol concentration. Less T201$_{peroxo}$ accumulated when the concentration of phenol was increased due to acceleration of its decay rate. A plot of the first derived decay rate constant (k_{decay1}) versus phenol concentration displayed saturation behavior (Figure 2B) and was fit (eq 1) to the processes depicted in Scheme 1, resulting in k_{sat} and K_d of 9 ± 2 s^{-1} and 10 ± 8 mM, respectively. The second decay process (k_{decay2}) was slightly perturbed by the presence of phenol, but with no clear dependence on its concentration, suggesting that T201$_{peroxo}$* may not react directly with substrate.

$$k_{obs}=k_o+\frac{k_{sat}[S]}{K_d+[S]} \quad (1)$$

To study further the arene-oxidizing mechanism of $T201_{peroxo}$, phenol-d_5 was used in the reaction of T201C $ToMOH_{red}D$ with dioxygen. Arene oxidation typically involves a hybridization change from sp^2 to sp^3 at a phenol carbon atom and, accordingly, an inverse kinetic isotope effect, KIE < 1, was observed (27). In this manner, the decay rate of $T201_{peroxo}$ arising from the use of phenol-h_5 versus phenol-d_5 and the resulting KIE can signal kinetic coupling to reaction with phenol. An inverse KIE of 0.82 ± 0.05, listed in Table 1, was derived, indicating that the decay of $T201_{peroxo}$ is kinetically linked to the arene oxidation. $T201_{peroxo}$ presumably attacks the arene ring in an electrophilic manner to generate an arene-oxide species (19). No KIE was observed for the following decay rate, $T201_{peroxo}^* \rightarrow ToMOH_{ox}$. As suggested above, $T201_{peroxo}^*$ is probably not involved in arene oxidation.

Reaction of T201G $ToMOH_{red}D$ with a solution of phenol in dioxygen-saturated buffer also led to the formation of $T201_{peroxo}$ (Figure 1C). The kinetic behavior of this reaction could not be monitored, however, because the oxidized product, catechol, binds to the diiron core, forming a Fe(III)-catecholate species with characteristic strong, interfering optical bands between 600–1020 nm that mask the optical feature of $T201_{peroxo}$ (28). Binding of catechol to the resting state enzyme after single turnover was also observed for the wild-type and T201S and T201C variants of ToMOH, but the decay rates of $T201_{peroxo}$ were much faster than the formation rates of Fe(III)-catecholate species so that optical changes at 675 nm, corresponding to the decay of $T201_{peroxo}$, were not obscured as they were for the T201G variant (data not shown).

Kinetic Solvent Isotope Effect in the Decay of $T201_{peroxo}$ in the Absence and Presence of Arene Substrates

A kinetic solvent isotope effect (KSIE) can be measured when deuterium oxide (D_2O) is used instead of H_2O as the solvent (29). A proposed chemical mechanism for $T201_{peroxo}$ decay in the absence of arene substrate is protonation of the hydroperoxo unit and subsequent release of hydrogen peroxide (19, 21). If $T201_{peroxo}$ requires a proton(s) in the decomposition pathway and the proton translocation step is coupled to decay of $T201_{peroxo}$, a KSIE ≥ 1 will be observed. The KSIE derived from the decay rates of $T201_{peroxo}$ in the presence of arene substrate, however, can be altered depending on whether or not the reaction is linked to arene oxidation, because a typical KIE for aromatic hydroxylation differs from that for proton translocation, as described above. We therefore derived KSIE values from the decay rates of $T201_{peroxo}$ in the absence and presence of phenol to distinguish the kinetically prevailing chemical step in $T201_{peroxo}$ decay and to provide an additional assessment of our previous conclusion that the more enhanced decay of $T201_{peroxo}$ upon addition of phenol is an indication of its kinetic competence.

To measure the KSIE for the decay of $T201_{peroxo}$, the reaction of T201C $ToMOH_{red}D$ with dioxy-gen was monitored in H_2O or D_2O buffer at 5 °C. Two consecutive decay rates of $T201_{peroxo}$ were observed in D_2O buffer, as previously seen in H_2O buffer. The k_{decay1} and k_{decay2} values measured in the two buffers returned $KSIE_{decay1}$ = 3.4 ± 0.3 and $KSIE_{decay2}$ = 6.5 ± 0.1 (Table 2). These large KSIE values for the decay process can imply multiple protons in a decay pathway (30), which presumably, for $T201_{peroxo}$, involve protonation of the peroxo moiety and release of H_2O_2. $KSIE_{decay}$ values ≥ 1 were observed for the T201S and T201G variants, 1.40 ± 0.11 and 10.6 ± 1.6, respectively (data not shown). $KSIE_{decay}$ values obtained from the decay rates of $T201_{peroxo}$ increase in the order T201S<T201C<T201G, possibly because of their increasingly poor ability to facilitate proton transfer during the decomposition of $T201_{peroxo}$.

Different $KSIE_{decay}$ results were obtained when experiments were conducted in the presence of phenol. KSIE studies in the presence of phenol were conducted only with T201C but not

the T201S and T201G variants. Although the $KSIE_{decay}$ in T201S ≥ 1, it is not large enough to permit an accurate value to be obtained in the presence of phenol. For the T201G variant, formation of the optical bands of Fe(III)-catecholate, as described previously, made it impossible to measure the $KSIE_{decay.}$ A solution of T201C $ToMOH_{red}D$ in either H_2O or D_2O buffer was therefore mixed with dioxygen-saturated buffer containing 10 mM phenol. Decay rates of $T201_{peroxo}$ in each buffer were measured, yielding $KSIE_{decay}$ values of 1.15 ± 0.06 and 2.1 ± 0.2 for two successive steps, respectively (Table 3). The dramatically reduced KSIE value for the first decay step compared to that determined in the absence of phenol, 3.4 ± 0.3, indicates that decay of $T201_{peroxo}$ is no longer entirely dependent on solvent protons but primarily involves an interaction of the peroxodiiron(III) intermediate with phenol. Therefore, the significant decrease in KSIE values due to introduction of the arene substrate supports the conclusion that $T201_{peroxo}$ is kinetically competent to hydroxylate phenol. The $KSIE_{decay}$ result for the second decay process (k_{decay2}) is also considerably perturbed by addition of phenol. Because $T201_{peroxo}$* does not probably react with phenol, as discussed above, the presence of phenol must trigger as yet unidentified reactions, for examples conformational changes, that contribute to the decay of $T201_{peroxo}$*.

Studies of T201X/I100W Variants (X = G, C, S, V)

As reported previously, I100 is located near the diiron active site where it helps to form a hydrophobic pocket (18). When I100 residue was mutated to I100W, the indole ring of the installed tryptophan approached the iron atoms, with Fe···C distances ranging from 6.0 to 11.9 Å (31). Addition of dioxygen to the reduced form of I100W ToMOH and To-MOD demonstrated that the variant activates O_2 at a rate similar to that observed for the wild type enzyme. The decay rate of $ToMOH_{peroxo}$ was accelerated, however, because the tryptophan residue serves as a substrate closely positioned near the active site, reacting with $ToMOH_{peroxo}$ to form diiron(III,IV) and I100W-radical species (31). The generation of the I100W-radical from $ToMOH_{peroxo}$ was nearly quantitative, and time-dependent RFQ/Mössbauer, EPR, and UV-vis spectroscopic studies revealed that the $ToMOH_{peroxo}$ decay rate corresponds to the formation rate of the I100W-radical species.

Based on these findings, T201X/I100W double mutants were prepared to examine the effect of the tryptophan residue on the decay rate of $T201_{peroxo}$ as well as the formation rate of the anticipated I100W-radical. I100W/T201X variants of ToMOH, prepared as described previously (X= S, G, C, V), all contained ~ 4 iron atoms/protein. When reduced T201S/I100W ToMOH and ToMOD were mixed with dioxygen-saturated buffer in the stopped-flow spectrophotometer at 4 °C, changes in the optical spectra at 675 nm and 500 nm originating from $T201_{peroxo}$ and I100W radical species, respectively, were observed (Figure 3 and Supporting Information Figure S1). From the data we computed formation and decay rates of $T201_{peroxo}$ and the I100W-radical species by fitting the optical changes to a function representing two consecutive, irreversible processes (Table 4). Both the formation and decay rate constants of $T201_{peroxo}$ and I100W-radical species in T201S/I100W were greatly perturbed compared to their values in T201S or I100W single variants (32). An accelerated decay rate of $T201_{peroxo}$ in T201S/I100W, compared to that in the T201S variant, implies that $T201_{peroxo}$ is on the reaction pathway of I100W oxidation, as discussed above for phenol oxidation. Three mechanisms were proposed to account for these data, as portrayed in Scheme 2. The increased $T201_{peroxo}$ decay rate rules out mechanism A in Scheme 2, whereby $T201_{peroxo}$ irreversibly decomposes to $ToMOH_{peroxo}$. If mechanism A were operative, only the decay rate of $ToMOH_{peroxo}$, but not that of $T201_{peroxo}$, would be accelerated by introduction of the arene substrate, tryptophan.

Both formation and decay of the I100W radical species are well fit by a single exponential function (Figure 3 and Table 4), which indicates that there is only one kinetically observable precursor, either $T201_{peroxo}$ or $ToMOH_{peroxo}$, but not both. These data therefore exclude

mechanism B in Scheme 2. The decay rate constant for $T201_{peroxo}$, 14.9 ± 0.4 s^{-1}, however, is much larger than the formation rate constant of the I100W radical species, 2.8 ± 0.1 s^{-1}, indicating that $T201_{peroxo}$ does not directly convert to the I100W radical species. These results indicate that an additional species, presumably $ToMOH_{peroxo}$, exists along the decay reaction pathway.

A third possible mechanism that we considered is one in which $T201_{peroxo}$ and $ToMOH_{peroxo}$ are in equilibrium with one another (Mechanism C, Scheme 2). This possibility is supported by the observed kinetic properties of the $T201_{peroxo}$ and I100W-radical intermediates in the T201S, I100W, and T201S/I100W variants. Although equilibrium between $T201_{peroxo}$ and $ToMOH_{peroxo}$ could potentially have complicated the kinetic analysis of $T201_{peroxo}$ decay, a single exponential function gave satisfactory estimates of the decay rate constants of $T201_{peroxo}$ in both the T201S and T201S/I100W variants (Table 4). This result indicates that the rate constant for conversion of $T201_{peroxo}$ to $ToMOH_{peroxo}$ (k_1) is much faster than the reverse rate constant (k_{-1}), Scheme 2C. The rapid forward rate presumably conveys kinetic competence to $T201_{peroxo}$ in arene oxidation, although this intermediate does not *directly* react with the substrate. Our observation that $T201_{peroxo}$ appears to be kinetically competent in arene oxidation is essentially due to its rapid conversion to $ToMOH_{peroxo}$ through the chemical equilibrium of Mechanism C in the presence of arene substrates.

A possible mechanism for the interconversion of $ToMOH_{peroxo}$ and $T201_{peroxo}$ is suggested in Scheme 3. A hydrogen-bonded proton on the hydroperoxo unit of $ToMOH_{peroxo}$ or on an oxygen atom of the adjacent glutamate (E231) in $T201_{peroxo}$ can easily shift between the two positions, as illustrated in the scheme. Such proton translocation can trigger reorganization of peroxo unit, altering the geometry of oxygenated diiron(III) species. The relative energetics of the two geometries, 1,1-hydroperoxodiiron(III) and 1,2-peroxodiiron(III), computed by QM/MM methods (23), indicated the energy difference between $ToMOH_{peroxo}$ and $T201_{peroxo}$ to be relatively small, as ~2.63 kcal/mol, and the occurrence of both intermediate species is therefore energetically plausible.

Introduction of I100W has a similar effect on the kinetic properties of $T201_{peroxo}$ in the other T201 variants. For T201C/I100W, formation of $T201_{peroxo}$ and the I100W radical species were monitored during the reaction of T201C/I100W $ToMOH_{red}D$ with O_2, as described for the T201S/I100W variant. Formation and decay of $T201_{peroxo}$ and the I100W-radical species in T201C/I100W monitored at 675 nm and 500 nm, respectively (Figure S2) and time-dependent traces were fit to a consecutive two exponential function without inclusion of $T201_{peroxo}$* in the decomposition pathway of $T201_{peroxo}$ to $ToMOH_{ox}$ (Table S1). Given that a consecutive three-exponential function was required to fit the trace of $T201_{peroxo}$ in the T201C single variant, the rapid decay of $T201_{peroxo}$ in the reaction with I100W residue does not proceed through $T201_{peroxo}$*. Acceleration of the decay rate of $T201_{peroxo}$ in T201C/I100W relative to the value in the T201C variant (k_{decay1}) again supports a mechanism in which $T201_{peroxo}$ is on the pathway of aromatic hydroxylation through equilibrium with $ToMOH_{peroxo}$ (Scheme 2C).

Both formation and decay rates of the I100W radical species in T201C/I100W are accelerated by comparison to those of I100W and T201S/I100W variants (Table S1). These kinetic characteristics of the I100W radical species in T201C/I100W can be perturbed if the local environment near the active sites is significantly altered. Previous studies with the I100W variant of ToMOH revealed that the formation and decay rates of I100W-radical species are pH-dependent (31). The rates are accelerated at high pH values, suggesting that deprotonation at tryptophan residue during formation and decay of I100W-radical species is preceded by a fast oxidation. Therefore, the acceleration of the formation and decay rates of

I100W-radical species in T201C/I100W relative to rates in the I100W or T201S/I100W variants possibly reflects local pH changes near the active site, induced by the T201C mutation. Because T201C is a poorer residue than T201 or T201S for promoting proton transfer, the T201C variant may experience an increase in local pH at the active site.

The T201G/I100W variant also generated the I100W-radical species during dioxygen activation (Table S1 and Figure S2). No $T201_{peroxo}$ species could be observed, however, probably because it reacts rapidly with I100W and does not accumulate to a detectable level.

Finally, dioxygen activation by the T201V/I100W variant was investigated (Table S1 and Figure S2). As expected from the T201V single variant study (21), $T201_{peroxo}$ was not detected in T201V/I100W. Possibly proton translocation, required for to generate $T201_{peroxo}$, is too slow; alternatively, formation of I100W-radical is too rapid to allow the intermediate to build up. Another possibility is that the T201V variant energetically disfavors formation of $T201_{peroxo}$ (21, 23). Reaction of T201V/I100W $ToMOH_{red}D$ with dioxygen also generated the I100W-radical species, possibly because the pectroscopically silent species, $ToMOH_{peroxo}$, formed and reacted with the tryptophan residue. The kinetic properties of the I100W-radical species in T201V/I100W are slightly different from those of I100W but rather similar to those of T201C/I100W, indicating that the local pH at the active site might similarly be perturbed owing to the presence of the hydrophobic valine side chain.

Quantification of I100W Radical Species in T201X/I100W Double Variants

The wild-type ToMOH displays half-sites reactivity, in which only one of the two diiron centers in the dimeric hydroxylase undergoes productive reactivity during single-turnover experiments. The other site can be reduced to the diiron(II) state but does not simultaneously form $ToMOH_{peroxo}$ upon introduction of O_2 (19). Half-sites reactivity is also consistently observed in reactions with phenol, whereby 50% catechol per diiron sites form during single turnover experiments (20, 33). In T201S, ~50% phenol oxidation was similarly measured during single-turnover, indicating that the serine variant retains half-sites reactivity (33). This property seems to be conserved in other T201 variants. Reactions of T201G $ToMOH_{red}D$ with dioxygen generated oxygenated intermediates at approximately half of the diiron centers. If half-sites reactivity is operative in all the T201G/C/V variants, approximately half of the enzyme present in solution would be able to oxidize phenol in single turnover experiments, but the yields were consistently lower than that value. This result contrasts with our findings for the wild-type and T201S variant. These findings indicate that decay of peroxodiiron(III) species is not tightly coupled to oxidation of hydrocarbon substrate when a hydroxyl group is lacking at position 201, presumably leading to release of hydrogen peroxide, rather than catechol, as an uncoupling product (34).

Single-turnover yields from the reaction of the internal I100W substrate were also determined for T201X/I100W double variants. The extinction coefficient of the I100W radical species at 500 nm is $\varepsilon_{500\ nm}$ = ~1500 cm^{-1} M^{-1}, based on Mössbauer and stopped-flow UV-vis data (31). Using this value, we were able to quantitate the amount of I100W-radical species generated in reactions of reduced T201X/I100W ToMOH and ToMOD with dioxygen. The I100W radical species produced was measured by taking into account of the individual formation and decay rate constants corresponding to the time-dependent spectral changes at 500 nm, as described previously (Table 5) (21). In I100W and T201S/I100W variants, ~50% of the I100W-radical species formed per diiron sites which is consistent with half-sites reactivity and ~50% of single turnover yields during phenol oxidation (20). By contrast, ~30% of I100W-radical species per diiron sites were generated in the T201C/G/V variants, even though ~50% of the diiron sites presumably reacted with dioxygen. The uncoupling chemistry in T201C/G/V variants is consistent with the single-turnover yields of these species during phenol oxidation. In addition, the results agree with the steady state

kinetics showing ~70–150-fold lower k_{cat}/K_M values for the T201C/G/V variants compared to the wild type and T201S enzymes. These results further support the notion that the hydroxyl group at position 201 site is necessary for efficient hydrocarbon oxidation (35).

Comparisons of Oxygenated Intermediates and Their Reactivities in ToMOH and sMMOH

Reaction of sMMOH with dioxygen consecutively generates three oxygenated intermediates, P*, P or H_{peroxo}, and Q, and the latter two species are capable of oxidizing hydrocarbon substrates (26, 36–38). H_{peroxo} and Q react with substrates through different mechanisms, with H_{peroxo} preferring more electron-rich substrates, such as propylene, ethyl vinyl ether, and diethyl ether, and operating by a two-electron transfer process. In contrast, Q favors one-electron transfer chemistry for methane oxidation (39). The promiscuous reactivity of sMMOH, therefore, can be attributed, at least in part, to the divergent reactions catalyzed by the two distinctive intermediates.

In contrast, ToMOH has evolved specifically to perform aromatic hydroxylation. A long and wide hydrophobic channel, ~ 6–10 Å by ~ 30–35 Å, is present only in toluene monooxygenases, where it most likely serves as the pathway for arene substrate access/product egress (18, 40). This structural feature may explain how ToMOH developed specificity for aromatic substrates. To perform aromatic hydroxylation, a high-valent oxygenated species like Q is unnecessary, because one-electron oxidation or C–H homolysis for arenes is not thermodynamically favorable owing to their high redox potentials and large C–H bond dissociation energies (41). An alternative mechanism is most likely operative in ToMOH. Oxidation of the arene can occur via two-electron transfer from substrates to an electrophilic oxidant, such as H_{peroxo} in sMMOH, the analogous species proposed for amine oxygenase (42, 43), and a hydroperoxoiron(III) intermediate in cytochrome P450 monooxygenase (41). The $ToMOH_{peroxo}$ intermediate in ToMOH therefore most likely shares the electronic and geometric structures of hydroperoxoiron(III) or peroxodiiron(III) species rather than those of Q in sMMOH.

A mechanism for the oxidation of arenes by $ToMOH_{peroxo}$ is proposed in Scheme 4. As previously reported (19), a Hammett plot for the oxidation of *para*-substituted phenols in ToMOH has a negative slope, consistent with the electrophilic character of $ToMOH_{peroxo}$. Electrophilic attack of the hydroperoxo unit in $ToMOH_{peroxo}$ on the arene ring can initiate the oxidation, followed by formation of an arene-oxide species, weakly bound to the diiron center. Addition of water and rearrangement can provide the arene product and return the resting state diiron site. A similar reaction with an arene substrate might be possible for $T201_{peroxo}$, although not kinetically feasible due to fast conversion to $To\text{-}MOH_{peroxo}$. Without such conversion, $T201_{peroxo}$ might participate in futile side reactions, becoming protonated with subsequent O–O bond cleavage and formation of a Q-type product with undesired reactivity.

CONCLUDING REMARKS

The present kinetic studies of $T201_{peroxo}$ in the absence and presence of external (phenol) or internal (tryptophan, as I100W) substrates clearly demonstrate that $T201_{peroxo}$ is kinetically on the reaction pathway of arene oxidation. Kinetic solvent isotope effects in the reaction of $T201_{peroxo}$ with phenol confirm this kinetic competence. Three reaction models were considered to account for the measured kinetics of $T201_{peroxo}$ and I100W-radical species formation and substrate reactivity. The only one that accounts for all of the experimental results requires that $T201_{peroxo}$ be in the equilibrium with $ToMOH_{peroxo}$. Acceleration in the decay rate of $T201_{peroxo}$ in the presence of arene substrates is therefore ascribed to the rapid conversion of $T201_{peroxo}$ to $ToMOH_{peroxo}$, the latter being the reactive species in arene oxidation.

Supplementary Material

Refer to Web version on PubMed Central for supplementary material.

Acknowledgments

We thank Dr. C. E. Tinberg for helpful comments on the manuscript.

References

1. Merkx M, Kopp DA, Sazinsky MH, Blazyk JL, Müller J, Lippard SJ. Dioxygen Activation and Methane Hydroxylation by Soluble Methane Monooxygenase: A Tale of Two Irons and Three Proteins. Angew Chem Int Ed. 2001; 40:2782–2807.
2. Wallar BJ, Lipscomb JD. Dioxygen Activation by Enzymes Containing Binuclear Non-Heme Iron Clusters. Chem Rev. 1996; 96:2625–2657. [PubMed: 11848839]
3. Solomon EI, Brunold TC, Davis MI, Kemsley JN, Lee SK, Lehnert N, Neese F, Skulan AJ, Yang YS, Zhou J. Geometric and Electronic Structure/Function Correlations in Non-Heme Iron Enzymes. Chem Rev. 2000; 100:235–349. [PubMed: 11749238]
4. Nordlund P, Eklund H. Structure and Function of the *Escherichia coli* Ribonucleoti-de Reductase Protein R2. J Mol Biol. 1993; 232:123–164. [PubMed: 8331655]
5. Fox BG, Shanklin J, Somerville C, Münck E. Stearoyl-acyl carrier protein Δ^9 de-saturase from *Ricinus communis* is a diiron-oxo protein. Proc Natl Acad Sci USA. 1993; 90:2486–2490. [PubMed: 8460163]
6. Xing G, Hoffart LM, Diao Y, Sandeep Prabhu K, Arne RJ, Reddy CC, Krebs C, Bollinger JM Jr. A Coupled Dinuclear Iron Cluster that Is Perturbed by Substrate Binding in *myo*-Inositol Oxygenase. Biochemistry. 2006; 45:5393–5401. [PubMed: 16634620]
7. Vu VV, Emerson JP, Martinho M, Kim YS, Münck E, Park MH, Que L Jr. Human Deoxyhypusine Hydroxylase, an Enzyme Involved in Regulating Cell Growth, Activates O_2 with a Nonheme Diiron Center. Proc Natl Acad Sci USA. 2009; 106:14814–14819. [PubMed: 19706422]
8. Choi YS, Zhang H, Brunzelle JS, Nair SK, Zhao H. *In vitro* reconstitution and crystal structure of *p*-aminobenzoate *N*-oxygenase (AurF) involved in aureothin biosynthesis. Proc Natl Acad Sci USA. 2008; 105:6858–6863. [PubMed: 18458342]
9. Behan KR, Lippard SJ. The Aging-Associated Enzyme CLK-1 is a Member of the Carboxylate-Bridged Diiron Family of Proteins. Biochemistry. 2010; 49:9679–9681. [PubMed: 20923139]
10. Lee SK, Fox BG, Froland WA, Lipscomb JD, Münck E. A Transient Intermediate of the Methane Monooxygenase Catalytic Cycle Containing an $Fe^{IV}Fe^{IV}$ Cluster. J Am Chem Soc. 1993; 115:6450–6451.
11. Liu KE, Wang D, Huynh BH, Edmondson DE, Salifoglou A, Lippard SJ. Spectroscopic Detection of Intermediates in the Reaction of Dioxygen with Reduced Methane Monooxygenase Hydroxylase from *Methylococcus capsulatus* (Bath). J Am Chem Soc. 1994; 116:7465–7466.
12. Liu KE, Valentine AM, Wang D, Huynh BH, Edmondson DE, Salifoglou A, Lip-pard SJ. Kinetic and Spectroscopic Characterization of Intermediates and Component Interactions in Reactions of Methane Monooxygenase from *Methylococcus capsulatus* (Bath). J Am Chem Soc. 1995; 117:10174–10185.
13. Lee SK, Lipscomb JD. Oxygen Activation Catalyzed by Methane Monooxygena-se Hydroxylase Component: Proton Delivery during the O-O Bond Cleavage Steps. Biochemistry. 1999; 38:4423–4432. [PubMed: 10194363]
14. Shu L, Nesheim JC, Kauffmann K, Münck E, Lipscomb JD, Que L Jr. An $Fe_2^{IV}O_2$ Diamond Core Structure for the Key Intermediate Q of Methane Monooxygenase. Science. 1997; 275:515–518. [PubMed: 8999792]
15. Tinberg CE, Lippard SJ. Revisiting the Mechanism of Dioxygen Activation in Soluble Methane Monooxygenase from *M. capsulatus* (Bath): Evidence for a Multi-Step, Proton-Dependent Reaction Pathway. Biochemistry. 2009; 48:12145–12158. [PubMed: 19921958]

16. Notomista E, Lahm A, Di Donato A, Tramontano A. Evolution of Bacterial and Archaeal Multicomponent Monooxygenases. J Mol Evol. 2003; 56:435–445. [PubMed: 12664163]
17. Leahy JG, Batchelor PJ, Morcomb SM. Evolution of the soluble diiron mo-nooxygenases. FEMS Microbiology Reviews. 2003; 27:449–479. [PubMed: 14550940]
18. Sazinsky MH, Bard J, Di Donato A, Lippard SJ. Crystal Structure of the Toluene/*o*-Xylene Monooxygenase Hydroxylase from *Pseudomonas stutzeri* OX1. J Biol Chem. 2004; 279:30600–30610. [PubMed: 15096510]
19. Murray LJ, Naik SG, Ortillo DO, García-Serres R, Lee JK, Huynh BH, Lippard SJ. Characterization of the Arene-Oxidizing Intermediate in ToMOH as a Diiron(III) Species. J Am Chem Soc. 2007; 129:14500–14510. [PubMed: 17967027]
20. Song WJ, Behan KR, Naik S, Huynh BH, Lippard SJ. Characterization of a Peroxodiiron(III) Intermediate in the T201S Variant of Toluene/*o*-Xylene Monooxygenase Hy-droxylase from *Pseudomonas* sp. OX1. J Am Chem Soc. 2009; 131:6074–6075. [PubMed: 19354250]
21. Song WJ, McCormick MS, Behan RK, Sazinsky MH, Jiang W, Jeffery L, Krebs C, Lippard SJ. Active Site Threonine Facilitates Proton Transfer During Dioxygen Activation at the Diiron Center of Toluene/*o*-Xylene Monooxygenase Hydroxylase. J Am Chem Soc. 2010; 132:13582–13585. [PubMed: 20839885]
22. Song WJ, Gucinski G, Sazinsky MH, Lippard SJ. 2011 Submitted.
23. Bochevarov AD, Li J, Song WJ, Lippard SJ, Friesner RA. Insights into different O_2-chemistry of methane and toluene monooxygenase hydroxylases. J Am Chem Soc ASAP. 2011
24. Cafaro V, Scognamiglio R, Viggiani A, Izzo V, Passaro I, Notomista E, Dal Piaz F, Amoresano A, Casbarra A, Pucci P, Di Donato A. Expression and purification of the recombinant subunits of toluene/*o*-xylene monooxygenase and reconstitution of the active complex. Eur J Biochem. 2002; 269:5689–5699. [PubMed: 12423369]
25. Murray LJ, García-Serres R, Naik S, Huynh BH, Lippard SJ. Dioxygen Activation at Non-Heme Diiron Centers: Characterization of Intermediates in a Mutant Form of Toluene/*o*-Xylene Monooxygenase Hydroxylase. J Am Chem Soc. 2006; 128:7458–7459. [PubMed: 16756297]
26. Beauvais LG, Lippard SJ. Reactions of the Peroxo Intermediate of Soluble Methane Monooxygenase Hydroxylase with Ethers. J Am Chem Soc. 2005; 127:7370–7378. [PubMed: 15898785]
27. Mitchell KH, Rogge CE, Gierahn T, Fox BG. Insight into the Mechanism of Aromatic Hydroxylation by Toluene 4-Monooxygenase by Use of Specifically Deuterated Toluene and *p*-Xylene. Proc Natl Acad Sci USA. 2003; 100:3784–3789. [PubMed: 12640145]
28. Cox DD, Que L Jr. Functional models for catechol 1,2-dioxygenase. The role of the iron(III) center. J Am Chem Soc. 1988; 110:8085–8092.
29. Quinn, DM.; Sutton, LD. Theoretical Basis and Mechanistic Utility of Solvent Isotope Effects, in Enzyme Mechanism from Isotope Effects. CRC Press; Boca Raton, FL: 1991.
30. Vidakovic M, Sligar SG, Li H, Poulos TL. Understanding the Role of the Essential Asp251 in Cytochrome P450cam Using Site-Directed Mutagenesis, Crystallography, and Kinetic Solvent Isotope Effect. Biochemistry. 1998; 37:9211–9219. [PubMed: 9649301]
31. Murray LJ, García-Serres R, McCormick MS, Davydov R, Naik SG, Kim SH, Hoff-man BM, Huynh BH, Lippard SJ. Dioxygen Activation at Non-Heme Diiron Centers: Oxidation of a Proximal Residue in the I100W Variant of Toluene/o-Xylene Monooxy-genase Hydroxylase. Biochemistry. 2007; 46:14795–14809. [PubMed: 18044971]
32. Dramatic changes due to the I100W residue in $T201_{peroxo}$ formation rate constants will be described separately.
33. Tinberg CE, Song WJ, Izzo V, Lippard SJ. Multiple Roles of Component Proteins in Bacterial Multicomponent Monooxygenases: Phenol Hydroxylase and Toluene/*o*-Xylene Monooxygenase from *Pseudomonas* sp. OX1. Biochemistry. 2011; 50:1788–1798. [PubMed: 21366224]
34. We attempted to quantitate the concentration of H_2O_2 in this reaction, but the catalase activity of ToMO led to an inaccurate measurement of H_2O_2 produced during single-turnover experiments.
35. Elsen NL, Bailey LJ, Hauser AD, Fox BG. Role for Threonine 201 in the Catalytic Cycle of the Soluble Diiron Hydroxylase Toluene 4-Monooxygenase. Biochemistry. 2009; 48:3838–3846. [PubMed: 19290655]

36. Valentine AM, Stahl SS, Lippard SJ. Mechanistic Studies of the Reaction of Reduced Methane Monooxygenase Hydroxylase with Dioxygen and Substrates. J Am Chem Soc. 1999; 121:3876–3887.

37. Brazeau BJ, Lipscomb JD. Kinetics and Activation Thermodynamics of Methane Monooxygenase Compound Q Formation and Reaction with Substrates. Biochemistry. 2000; 39:13503–13515. [PubMed: 11063587]

38. Tinberg CE, Lippard SJ. Oxidation Reactions Performed by Soluble Methane Monooxygenase Hydroxylase Intermediates H_{peroxo} and Q Proceed by Distinct Mechanisms. Biochemistry. 2010; 49:7902–7912. [PubMed: 20681546]

39. Baik MH, Gherman BF, Friesner RA, Lippard SJ. Hydroxylation of Methane by Non-Heme Diiron Enzymes: Molecular Orbital Analysis of C-H Bond Activation by Reactive Intermediate Q. J Am Chem Soc. 2002; 124:14608–14615. [PubMed: 12465971]

40. Bailey LJ, McCoy JG, Phillips J, George N, Fox BG. Structural Consequences of Effector Protein Complex Formation in a Diiron Hydroxylase. Proc Natl Acad Sci. 2008; 105:19194–19198. [PubMed: 19033467]

41. Meunier B, de Visser SP, Shaik S. Mechanism of Oxidation Reactions Catalyzed by Cytochrome P450 Enzymes. Chem Rev. 2004; 104:3947–3980. [PubMed: 15352783]

42. Korboukh VK, Li N, Barr EW, Bollinger JM Jr, Krebs C. A Long-Lived, Substrate-Hydroxylating Peroxodiiron(III/III) Intermediate in the Amine Oxygenase, AurF, from *Streptomyces thioluteus*. J Am Chem Soc. 2009; 131:13608–13609. [PubMed: 19731912]

43. Li N, Korboukh VK, Krebs C, Bollinger JM Jr. Four-electron oxidation of p-hydroxylaminobenzoate to *p*-nitrobenzoate by a peroxodiferric complex in AurF from *Streptomyces thioluteus*. Proc Natl Acad Sci USA. 2010; 107:15722–15727. [PubMed: 20798054]

(A)

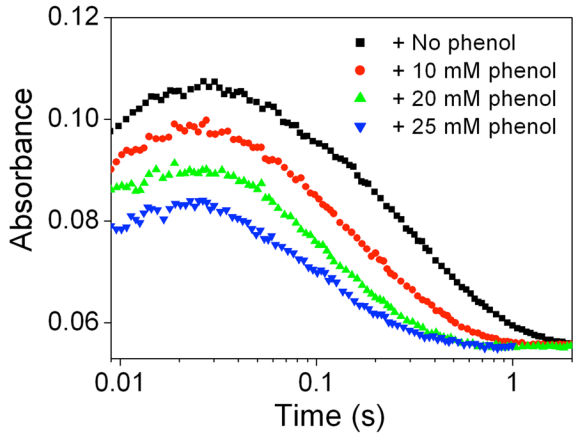

(B)

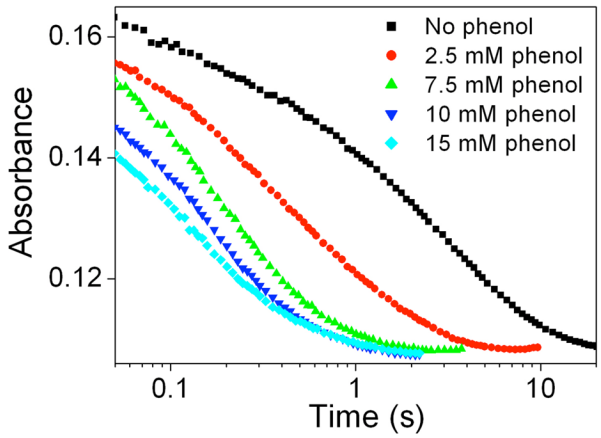

(C)

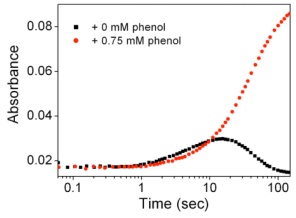

Figure 1.

Trace of $T201_{peroxo}$ at 675 nm in the absence and presence of phenol in T201 variants of To-MOH. (A) T201S (B) T201C (C) T201G.

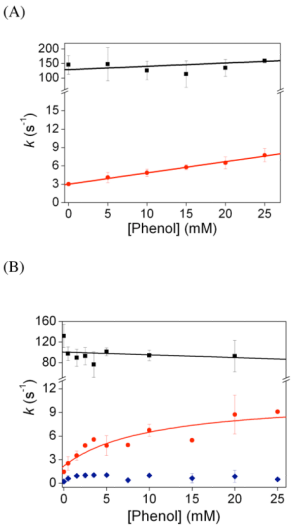

Figure 2.

Plots of $T201_{peroxo}$ formation and decay rate constants versus phenol concentrations in the reaction of T201X $ToMOH_{red}D$ with phenol in dioxygen-saturated buffer. (A) T201S (B) T201C Formation and decay rates are represented with black squares and red circles, respectively. For T201C variant, second decay rate constants are shown as navy diamonds. Formation and decay rate constants are plotted with either a linear or a saturation function.

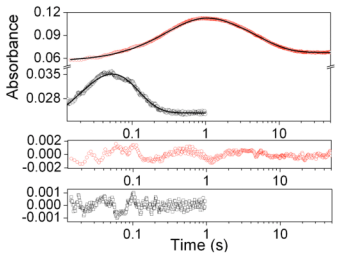

Figure 3.

Time-dependent optical changes in the reaction of T201S/I100W ToMOH$_{red}$D with dioxygen at 675 nm (black squares) and 500 nm (red circles) and fit to a function representing two consecutive, irreversible processes. Fitting results are represented as blue lines in spectra and with residuals shown below.

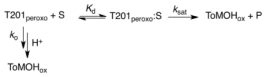

Scheme 1.

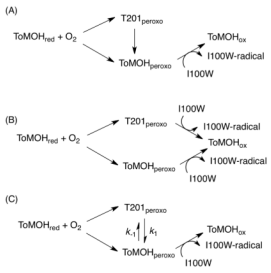

Scheme 2.

Reaction Models for the Formation and Decay of $T201_{peroxo}$ during Dioxygen Activation of T201X/I100W ToMOH.

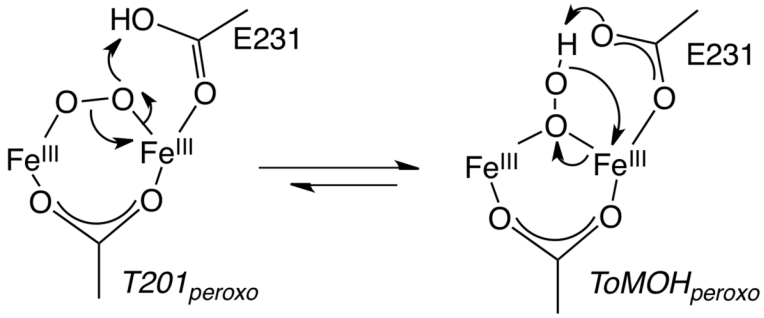

Scheme 3.
Proposed Mechanism for the Interconversion of $T201_{peroxo}$ and $ToMOH_{peroxo}$.

Scheme 4.
Proposed Mechanism of Aromatic Hydroxylation by $ToMOH_{peroxo}$ and $T201_{peroxo}$ in T201 Variants of ToMOH.

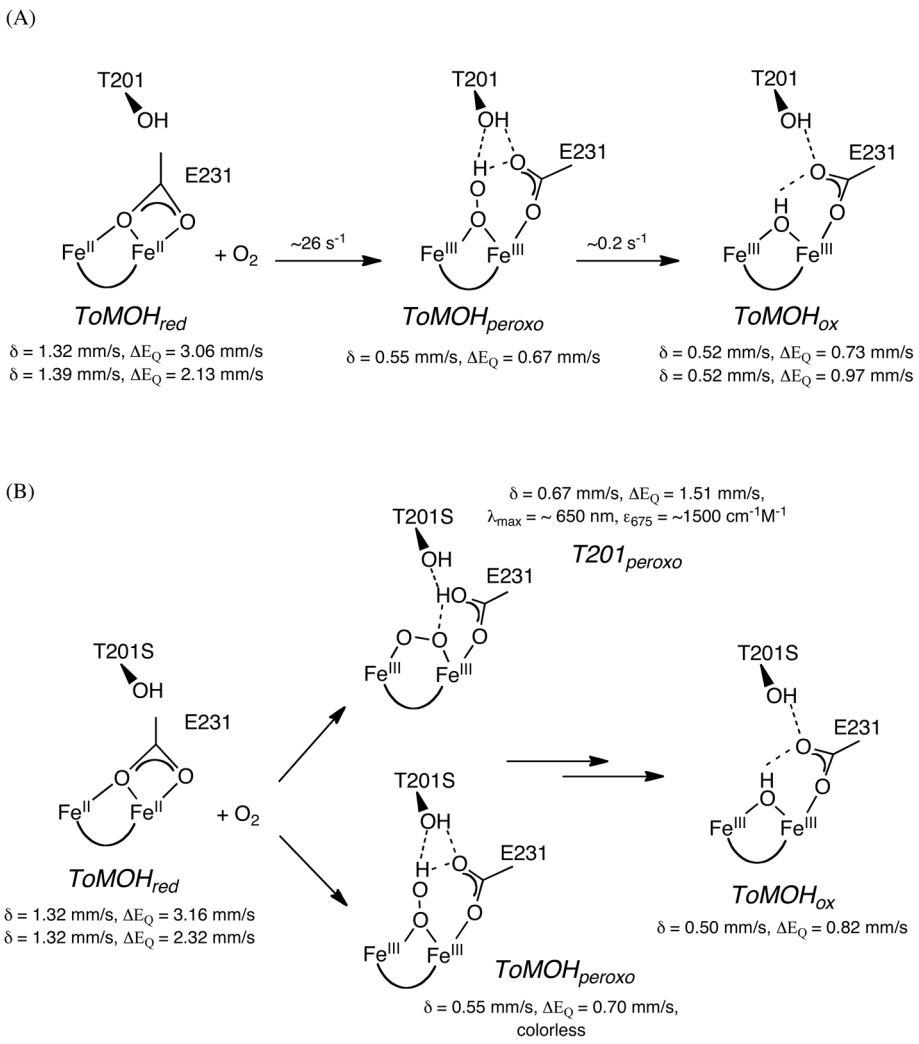

Chart 1.
Dioxygen Chemistry in (A) Wild-Type ToMOH and (B) the T201S Variant of ToMOH at 4 °C, pH 7.

Table 1

Consecutive Decay Kinetic Constants for $T201_{peroxo}$ in the Reaction of T201C $ToMOH_{red}D$ with Phenol in Dioxygen-Saturated Buffer.

	phenol-h_5	**phenol-d_5**	**KIE**
k_{decay1} (s^{-1})	7.2 ± 0.3	8.7 ± 0.3	0.82 ± 0.05
k_{decay2} (s^{-1})	2.2 ± 0.2	2.1 ± 0.2	1.1 ± 0.1

Table 2

Consecutive Decay Rate Constants and KSIE Values for $T201_{peroxo}$ in the Reaction of T201C $ToMOH_{red}D$ with Dioxygen in H_2O or D_2O Buffer.

	H_2O	D_2O	KSIE
k_{decay1} (s^{-1})	1.9 ± 0.1	0.557 ± 0.007	3.4 ± 0.3
k_{decay2} (s^{-1})	0.241 ± 0.004	0.0382 ± 0.0001	6.5 ± 0.1

Table 3

Consecutive Decay Rate Constants and KSIE Values for $T201_{peroxo}$ in the Reaction of T201C $ToMOH_{red}D$ with Dioxygen and 10 mM Phenol in H_2O or D_2O Buffer.

	H_2O	D_2O	KSIE
k_{decay1} (s^{-1})	7.2 ± 0.3	6.26 ± 0.07	1.15 ± 0.06
k_{decay2} (s^{-1})	2.2 ± 0.2	1.02 ± 0.03	2.1 ± 0.2

Table 4

Formation and Decay Rate Constants for $T201_{peroxo}$ and W-radical Intermediates Generated During Dioxygen Activation of I100, T201S, and T201S/I100W $ToMOH_{red}D$.

	I100W	T201S	T201S/I100W
$T201_{peroxo}$	nd[a]	$k_{form} = 88 \pm 7\ s^{-1}$ $k_{decay} = 3.1 \pm 0.3\ s^{-1}$	$k_{form} = 55 \pm 14\ s^{-1}$ $k_{decay} = 14.9 \pm 0.4\ s^{-1}$
I100W-radical	[b] $k_{form} = 0.804 \pm 0.001\ s^{-1}$ [b] $k_{decay} = 0.054 \pm 0.002\ s^{-1}$	nd[a]	$k_{form} = 2.88 \pm 0.12\ s^{-1}$ $k_{decay} = 0.19 \pm 0.01\ s^{-1}$

[a] Not determined.

[b] Taken from ref. 31.

Table 5

Quantification of I100W-Radical Species Generated in T201X/I100W ToMOH.

	I100W	T201S/I100W	T201C/I100W	T201G/I100W	T201V/I100W
Coupling (%)	55 ± 1%	49 ± 1%	36 ± 2%	38 ± 1%	31 ± 2%